NREL/TP-441-7077 • UC Category: 1213 • DE94011862



# Using Digital Filtering Techniques as an Aid in Wind Turbine Data Analysis

Teresa Young

*Prepared for*
*AIAA Region V Student Conference*
*April 21–24, 1993*
*Fort Collins, Colorado*


National Renewable Energy Laboratory
1617 Cole Boulevard
Golden, Colorado 80401-3393
A national laboratory of the U.S. Department of Energy
Managed by Midwest Research Institute
for the U.S. Department of Energy
under contract No. DE-AC36-83CH10093

Prepared under Task No. WE418120



November 1994

**NOTICE**



Available to DOE and DOE contractors from:
Office of Scientific and Technical Information (OSTI)
P.O. Box 62
Oak Ridge, TN 37831
Prices available by calling (615) 576-8401

Available to the public from:
National Technical Information Service (NTIS)
U.S. Department of Commerce
5285 Port Royal Road
Springfield, VA 22161
(703) 487-4650

## DISCLAIMER

Portions of this document may be illegible in electronic image products. Images are produced from the best available original document.

# USING DIGITAL FILTERING TECHNIQUES AS AN AID IN WIND TURBINE DATA ANALYSIS

Teresa Young
BioServe Space Technologies, University of Colorado at Boulder, CB 429, Boulder Colorado 80309-0429, (303)492-1005.

## Abstract

Research involving very large sets of digital data is often difficult due to the enormity of the database. In the case of a wind turbine operating under varying environmental conditions, determining which data are representative of the blade aerodynamics and which are due to transient flow ingestion effects or errors in instrumentation, operation, and data collection is of primary concern to researchers. The National Renewable Energy Laboratory in Golden, Colorado collected extensive data on a downwind horizontal axis wind turbine (HAWT) during a turbine test project called the Combined Experiment. A principal objective of this experiment was to provide a means to predict HAWT aerodynamic, mechanical, and electrical operational loads based upon analytical models of aerodynamic performance related to blade design and inflow conditions. In a collaborative effort with the Aerospace Engineering Department at the University of Colorado at Boulder, a team of researchers has evolved and utilized various digital filtering techniques in analyzing the data from the Combined Experiment.

A preliminary analysis of the data set was performed to determine how to best approach the data. A filter based upon data norms was employed to identify and correct anomalous data, most of which appeared to arise from equipment malfunctions. Likewise, a filter was utilized to smooth noise in the data. Thereafter, a determination of the stochastic distribution of the data was made. Several different filtering techniques were then employed to obtain a reduced data set based upon this preliminary analysis. The reduced data set emphasized selection of inflow conditions such that the aerodynamic data could be compared directly to wind tunnel data obtained for the same airfoil design as used for the HAWT's blades. It will be shown that this reduced data set has yielded valid, reproducible results that a simple averaging technique or a random selection approach cannot achieve. These findings provide a stable baseline against which operational HAWT data can be compared.

## Introduction

Wind is a readily available, non-polluting renewable source of energy. Yet, wind energy currently accounts for a very small percentage of power produced in the United States because costs remain comparatively high. A major problem with wind energy costs is that wind turbines have shorter lifetimes than that predicted by wind tunnel tests. Wind turbines, designed to last 20 to 30 years, often break after only 2 to 3 years in the field. It is suspected that environmental aerodynamic effects are responsible for large transient loads which damage the wind turbines and their blades. If these effects were fully characterized and understood, turbines could be designed to minimize the damage now caused by the unexpectedly large transient loads. Such improvements could reduce the costs of wind energy to half of the current levels, making wind energy competitive in cost to conventional energy sources.

A primary focus of the National Renewable Energy Laboratory (NREL) is the study of wind energy in an attempt to maximize energy production, minimize cost, and eliminate the associated problems. Currently wind tunnel tests are used to predict the loads and thus the lifetimes of the blades, gearboxes, and generators but are conducted only under fairly constant, low turbulence conditions. However, the operational environment of wind turbines is quite different than that in a wind tunnel. They must operate across a variety of environmentally-induced inflow conditions and even within turbine-induced inflow conditions such as those experienced in wind farms.

To bridge the gap between wind tunnel testing and wind turbine operational aerodynamics, NREL designed the Combined Experiment. This experiment consists of a highly

instrumented horizontal axis wind turbine (HAWT) operating at Rocky Flats, a few miles south of Boulder, Colorado. The extensive data obtained from the Combined Experiment must be evaluated to (1) reveal the operating characteristics encountered by HAWTs in the field and (2) to discern the relations between wind tunnel tests and field runs.

## Test Setup

The Combined Experiment consists of a modified Grumman Wind Stream 33 downwind HAWT with a rotor diameter of 10.1 meters. Figure 1 is a diagram of the turbine and the Vertical Plane Array (VPA). The VPA, located 12 meters upwind from the turbine, gathers data on inflow magnitude and direction via 13 anemometers. The turbine rotates at a constant speed of 72 rpm and has three 45.7 centimeter constant chord blades with no twist. The simple, rectangular geometry of these blades presumably simplifies the aerodynamic analyses.

The Combined Experiment is currently the most highly instrumented wind turbine in the world. Data is taken for 190 measured channels from the turbine, the VPA, and two meteorological towers. This data is broken up into four broad categories: aerodynamic, environmental and inflow, structural, and operational data. Figure 2 lists all of the measured data channels grouped according to location and the rate at which each measurement was sampled.

One of the three turbine blades is highly instrumented to provide high quality aerodynamic data. The instrumented blade has 109 pressure taps distributed between the four spanwise locations of 30%, 47%, 63%, and 80%

COMBINED EXPERIMENT TEST SETUP

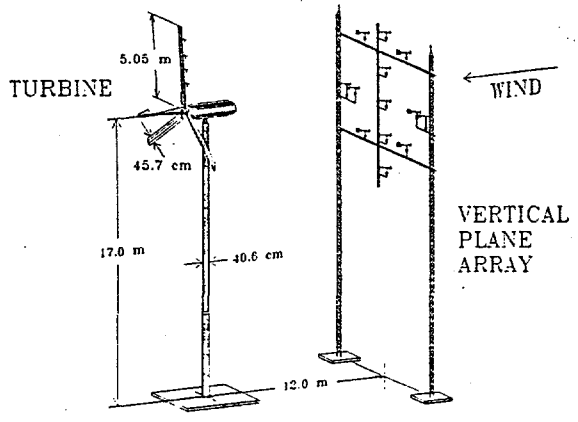


**Figure 1:** Three-dimensional view of the Grumman Wind Stream 33 horizontal axis wind turbine and the vertical plane array utilized in the Combined Experiment.

**Turbine Rotor**
520.83 Hz Sample Rate

| Pressure Measurement Locations (ESP-32 transducers) | Upper Surface | Lower Surface |
|---|---|---|
| 30%Span | 15 | 10 |
| 35.6% Span | 2 | |
| 41.1% Span | 2 | |
| 47% Span | 18 | 10 |
| 52.2% Span | 2 | |
| 57.8% Span | 2 | |
| 63% Span | 18 | 10 |
| 68.9% Span | 2 | |
| 74.4% Span | 2 | |
| 80% Span | 18 | 10 |

4 Total Pressure Probes (34%,50.6%, 67.3%, 86% span)

Force Measurements
- 4 Root Flap Bending
- 5 Flap Bending (20%, 40%, 50%, 70%, 90% span)
- 3 Edge Bending (0%, 50%, 70% span)
- 3 Blade Torque (0%, 20%, 50% span)
- 2 Low Speed Shaft Bending
- 2 Low Speed Shaft Torque

Atmospheric Condition
- 1 Absolute Pressure Reference

Miscellaneous Measurements
- 4 Angle of Attack (34%, 50.6%, 67.3%, 86%)
- 1 Pitch Angle

**Vertical Plane Array (VPA)**
69.44 Hz Sample Rate

Wind Speed
- 11 Prop Vane Anemometers
- 2 Bi-Vane Anemometers

Wind Direction
- 1 Prop Vane Anemometer
- 2 Bi-Vane Anemometers

Wind Angle
- 2 Bi-Vane Anemometers

**Local MET Tower**
277.78 Hz Sample

Wind Speed
- 3 Sonic Anemometers
- 2 X-Film Anemometers

**Nacelle & Tower**
277.78 Hz Sample Rate

Force Measurements
- 1 Yaw Moment
- 2 Tower Bending

Miscellaneous Measurements
- 1 Low Speed Shaft Azimuth Angle
- 1 Yaw Angle
- 1 Generator Power

**Far Met Tower**
34.72 Hz Sample Rate

Wind Speed
- 4 Teledyne Cup Anemometers (at heights of 5 m, 10 m, 20 m, 50 m)

Wind Direction
- 4 Teledyne Vane Anemometers (at heights of 5 m, 10 m, 20 m, 50 m)

Atmospheric Conditions
- 2 Air Temperature (at heights of 5 m and 50 m)
- 1 Barometric Pressure

**Figure 2:** Table summarizing measured data channels based on measurement location and sampling rate.

span. There are approximately 28 taps located at each span location spaced chordwise along both the upper and lower surfaces. In addition, there are two taps located at each of six intermediate span locations on the upper surface to further characterize the flow in the spanwise direction. The pressure taps allow for a three-dimensional instantaneous realization of the pressure acting upon the entire blade, upper and lower surfaces.

A dynamic pressure probe is mounted slightly outboard of each of the four primary pressure tap span locations protruding from the leading edge of blade. These provide data about the local dynamic pressure, and hence, the local velocity at each span location. Also, mounted with the dynamic pressure probes are angle of attack sensors that consist of a dynamically balanced flag that aligns itself with the flow to indicate local angle of attack.

Inflow data is collected primarily through the VPA. Its 11 propvane and 2 bi-vane anemometers are arranged in two concentric circles and allow a characterization of the inflow magnitude and direction over the entire rotor disk. A local meteorological (MET) tower 10 meters from the VPA provides additional velocity information, including turbulence levels. Finally, the far MET tower, located 1 km northwest of the experiment site, provides far-field inflow data as well as atmospheric information such as temperature and pressure.

To quantify the effect that the aerodynamic forces have on the turbine, strain gages provide force measurements on the blades, nacelle, tower, and other locations. Blade measurements include root flap bending moments on all three blades and flap bending moments measured at five spanwise locations, edge bending, and blade torque on the instrumented blade. Force measurements on the nacelle and tower include yaw moment and tower bending.

Finally, measurements are taken to help characterize the operational state of the turbine. These include azimuth angle (the position within a rotational cycle), yaw angle, and generator power.

Supplementing the measured data are 44 derived channels of data that have been calculated from the measured channels. Typically, these channels contain information that has been integrated over a number of measurements, such as pressure taps. For instance, the normal and tangential force components, $C_n$ and $C_t$, represent the integrated pressure over the blade at each span location, and the disc average wind speed is an average of eight of the VPA anemometers.

All data channels recorded on the turbine rotor, including all pressure measurements and blade moments, were sampled at 521 Hz. The remaining channels were sampled at rates varying from 35 Hz to 278 Hz and were extrapolated to 521 Hz. Data was collected across 59 separate test episodes, each of approximately 5 minutes duration. The resulting data, approximately 9 gigabytes, was recorded in binary format on 30 optical disks. While this established an extensive database for studying wind turbine aerodynamics and their associated structural effects over a wide range of operational conditions, the sheer volume of data required that special processing and analyzation techniques be employed. For a more thorough description of the test setup consult Butterfield and Nelsen [1] and Butterfield et al [2].

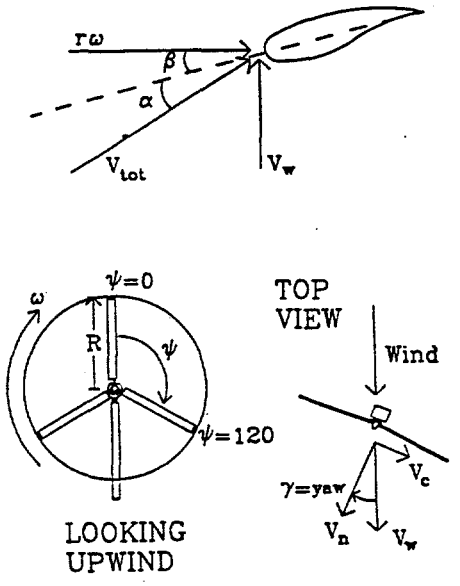


**Figure 3:** Wind turbine geometric relationships and experimental nomenclature.

## Nomenclature

The diagrams in Figure 3 show the researcher's nomenclature. Looking upwind at the rotating blade, $\psi$, the azimuth angle, is the angle the instrumented blade is positioned clockwise from 0° (straight up). A cycle is defined as one rotation of the instrumented blade from 0° to 360°. R, the blade radius, is defined as the length from the tip of the blade to center hub. The top view shows the wind vector and its components. $V_W$ represents the freestream velocity. $V_W$ can be decomposed into $V_n$, the normal velocity, which is perpendicular to the plane of the blades, and $V_C$, the crossflow velocity, which is in the plane of blade rotation. The yaw, $\gamma$, is the angle between $V_n$ and $V_W$.

The cross-sectional view of the blade shows the total local velocity as seen by the blade and its components. The rotational velocity is $r\omega$, where r is the radius of the blade from the center of the hub to the cross-sectioned area, and $\omega$ the rotational frequency, which is a constant $2.4\pi$ rad/sec. The total velocity, $V_{tot}$, is the vector sum of $V_W$ and $r\omega$. The blade pitch, $\beta$, was set at 12° for the Combined Experiment. $\alpha$ is the angle of attack of the blade.

Angle of attack defines the blade orientation with respect to the incoming flow and is used in wind tunnel tests to characterize blade aerodynamic performance. However, unlike in the wind tunnel, angle of attack on a turbine blade is not dependent solely upon geometric orientation. On a rotating blade, angle of attack is a function of inflow velocity, span location and rotational frequency. In addition, inflow velocity, and hence, angle of attack, are affected by operation at yaw angles other than 0° and local flow perturbations such as the tower shadow. Angle of attack is related to the inflow and rotational velocities by the folowing formula:

$$\alpha = \tan^{-1} (V_W / r\omega) - \beta.$$

Theoretical angle of attack at 0° yaw is plotted as a function of velocity for all four span locations in Figure 4. This figure illustrates that an increase in velocity leads to an increase in angle of attack for a given span location. Likewise, at any velocity the angle of attack increases as you move further inboard.

## Problem Statement

An empirical baseline characterizing the blade aerodynamic performance is required for assesing overall operational HAWT regimes and corroborating HAWT data with known wind tunnel data. The independent variables defining an aerodynamic event include freestream wind velocity, effective angle of attack ,and turbulence levels. The blade performance is often defined by effective angle of attack and the pressure distributions produced for well-behaved flow velocities. Thus, all aerodynamic effects are dependent upon the inflow conditions.

When this study first began, the data had been binned by average velocity and the aerodynamic data had been averaged together. However, the stochastic distribution of the data suggests that binning and averaging resulted in poor resolution both for velocity and yaw as well as for the recorded aerodynamic effects. Clearly, the time varying conditions were not well resolved. For example, the tower shadow effect, the wind velocity deficit behind the turbine tower, is an inflow condition which affects blade performance but is currently not resolved. The binned cycles reflected such variance in inflow conditions that much of the

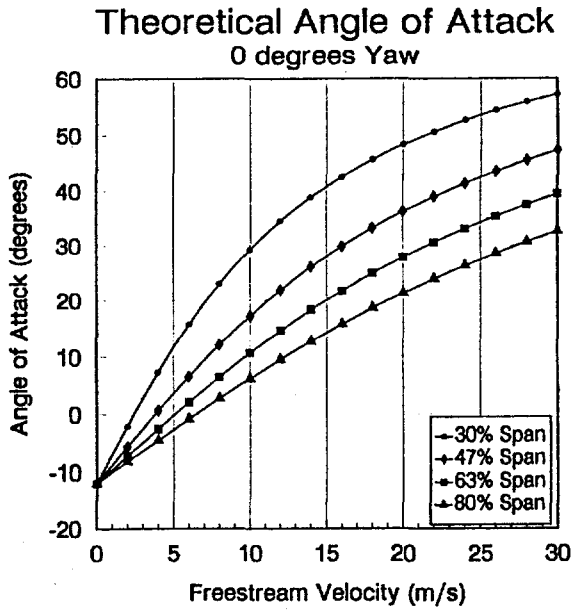


**Figure 4:** Theoretical angle of attack based on freestream velocity at zero degrees yaw for 30%, 47%, 63%, and 80% span.

aerodynamics about the blade could not be reasonably discerned or compared to relevant wind tunnel test conditions. Therefore, since yaw and velocity were likely to have the greatest effects upon the dynamics of the blade, the data were systematically characterized and plotted by mean yaw and velocity. Figure 5 shows the distribution of the 5 minute test episodes with regards to both overall mean velocity and yaw. Some ranges in the matrix contain several 5 minutes episodes of data while others have no data. The complete set contains the most data for yaw angles in the range of -9° to 3° and for wind velocities of 5 to 11 m/s. Several values in the yaw-velocity matrix are not available. For a velocity greater than 17 m/s, only a yaw angle in the range of -9° to 3° is represented, and in the case of 9° to 15° yaw, only velocities in the 5 to 8 m/s range are available.

A closer look at the data set reveals that even in the same mean velocity and mean yaw ranges, there can be wide variance in the rotational cycle distributions of these variables. Figure 6 contains histograms of the cycle velocities for two five minute episodes with similar mean velocities and yaws. Tape d072011 has a mean velocity of 11.3 ± 3.6 m/s and mean yaw of -5.8° ± 13.3°. Individual cycles within this set show a range of velocity, from 3 m/s to 18 m/s. Many cycles appear to show 10 m/s velocities. The velocity distribution within this test episode is quite different from that of Tape d072041.

**Combined Experiment Inflow Data Distribution**

**Mean Velocity and Standard Deviation**

Average Velocity (m/s)

| Average Yaw (degrees) | < 5 | 5 - 8 | 8 - 11 | 11 - 14 | 14 - 17 | > 17 | Row Ave |
|---|---|---|---|---|---|---|---|
| -15 - -9 | - | 7.4 ± 1.7 | 10.3 ± 3.0 | - | - | - | 8.3 ± 2.5 |
| -9 - -3 | 4.2 ± 1.4 | 6.4 ± 1.5 | 9.2 ± 1.9 | 12.8 ± 2.9 | 14.8 ± 2.8 | 17.8 ± 3.2 | 11.4 ± 4.7 |
| -3 - 3 | 4.7 ± 1.5 | 7.3 ± 1.3 | 9.3 ± 1.6 | 12.4 ± 2.6 | 15.5 ± 2.8 | - | 9.5 ± 3.6 |
| 3 - 9 | - | 6.8 ± 1.5 | - | - | 14.2 ± 3.7 | - | 8.3 ± 3.6 |
| 9 - 15 | - | 7.7 ± 1.4 | - | - | - | - | 7.7 ± 1.4 |
| | 4.6 ± 1.5 | 7.0 ± 1.5 | 9.3 ± 1.8 | 12.6 ± 2.8 | 15.0 ± 2.9 | 17.8 ± 3.2 | 10.1 ± 4.2 |
| | Column Averages | | | | | | Total |

**Mean Yaw and Standard Deviation**

Average Velocity (m/s)

| Average Yaw (degrees) | < 5 | 5 - 8 | 8 - 11 | 11 - 14 | 14 - 17 | > 17 | Row Ave |
|---|---|---|---|---|---|---|---|
| -15 - -9 | - | -15.4 ± 15.3 | -9.4 ± 21.3 | - | - | - | -13.5 ± 17.6 |
| -9 - -3 | -8.2 ± 20.2 | -5.3 ± 14.4 | -4.6 ± 11.8 | -4.6 ± 10.9 | -4.2 ± 11.6 | -3.6 ± 12.7 | -4.7 ± 12.7 |
| -3 - 3 | -0.3 ± 9.7 | 0.0 ± 11.3 | -1.3 ± 11.6 | -1.1 ± 12.9 | -2.1 ± 11.9 | - | -0.9 ± 11.6 |
| 3 - 9 | - | 3.8 ± 12.6 | - | - | 5.6 ± 13.7 | - | 4.2 ± 12.8 |
| 9 - 15 | - | 13.5 ± 20.9 | - | - | - | - | 13.5 ± 20.9 |
| | -2.9 ± 14.6 | -1.4 ± 14.6 | -3.0 ± 12.7 | -3.2 ± 11.8 | -2.2 ± 12.4 | -3.6 ± 12.7 | -2.4 ± 13.3 |
| | Column Averages | | | | | | Total |

**Figure 5:** Data distribution with respect to mean velocity and mean yaw over all 5 minute test episodes.

Although this second test episode has a mean velocity of 11.6 ± 3.7 m/s and a mean yaw of -5.4° ± 14.6°, its cycle by cycle distribution of velocities clearly has a central mode at around 9 m/s and velocity range from 6 to 21 m/s. Neither plot shows a stochastically normal distribution and, therefore, neither would be well characterized by an averaging approach. Thus events that might seem to yield similar results do not.

A method to limit yaw and velocity was needed in order to establish a baseline to define the turbine aerodynamic effects. Due to the dynamic nature of the environmental inflow conditions, even episodes of the same apparent

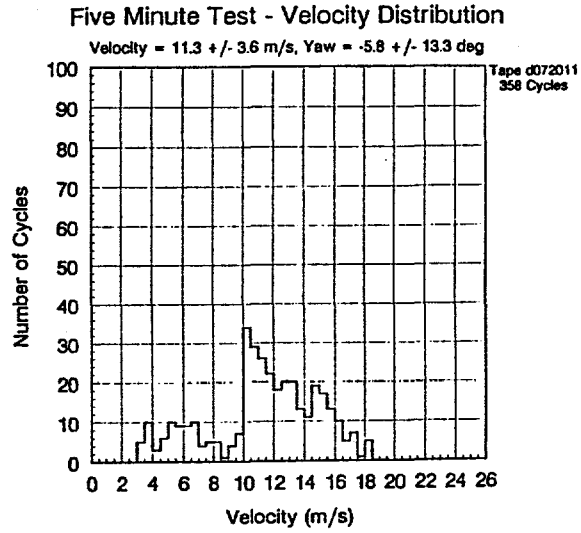


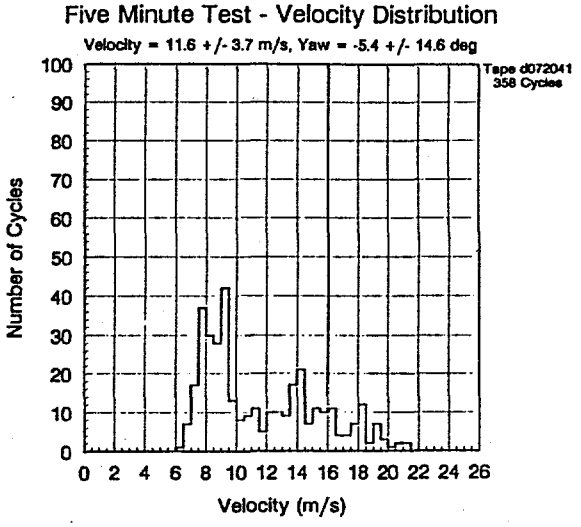


**Figure 6:** Velocity distribution histograms for single cycles over two separate 5 minute test episodes with similar mean velocities and yaws.

yaw and velocity could yield very different aerodynamic effects, as can be seen in Figure 7. Figure 7 shows the upper blade surface pressure distribution at the 30% span location for two different cycles of 20 m/s freestream wind velocity and approximately 0° yaw. The cycles are from the same data run and occur only 0.83 seconds apart and yet show very different pressure profiles. The blade on cycle 355 experienced a greater pressure differential peak at a slightly different azimuth angle than did the blade during cycle 353. Cycle 353 also has a secondary pressure differential peak that is evident from about 30% - 40% chord to 80% chord. If these two pressure distributions were simply averaged, much of the essential blade aerodynamics would be lost. Obviously, a simple binning and averaging of similar velocity and yaw cases would not necessarily indicate the aerodynamic events.

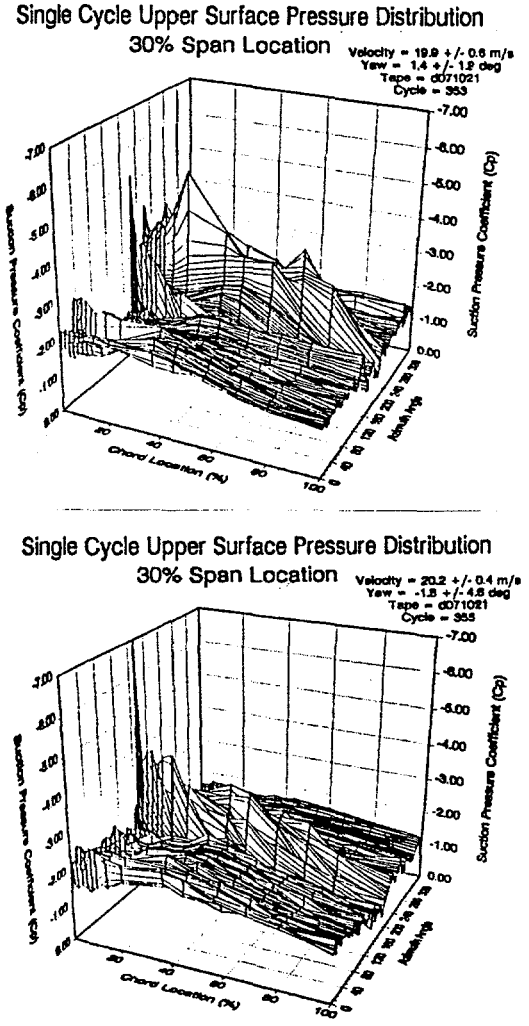


**Figure 7:** Two single cycle upper surface pressure profiles at 30% span illustrating the vast differences that may exist even between cycles with similar velocities and yaws.

## Analysis

The data shows variance due to changing inflow conditions such as rapid variations in yaw and velocity and rapid interactions with the tower wake. So, to simplify analysis, the cycles which did not show large variations in these conditions were the focus of study. Thus, a baseline by which to measure the effects of these large variations could be established. The working hypothesis was that constant inflow conditions should lead to consistent data. And, these data should share certain characteristics with those obtained in wind tunnel tests. A method was needed to limit a working data set to similar, reproducible aerodynamic conditions events. Two different approaches were taken. One was a correlational approach which found temporally consistent cycles based on pressure profiles, while the other approach identified cycles with inflow conditions that remained relatively constant across several consecutive turbine blade rotation cycles.

Due to the dynamic nature of the inflow conditions and the size of the whole data set, the data were first grouped into 50 cycles sets which were subsequently rank ordered in terms of yaw and freestream velocity variance for a selection of velocities over the operational range of the turbine (5, 8.5, 10, 15, 20 m/s) and 0° yaw. Analysis was limited to 0° yaw since yawed operation introduces cyclic variations in angle of attack. The set identified as representing the most consistent inflow conditions, that is, the one with the smallest variance in velocity and yaw was chosen for each of the five velocity cases.

Before the data from these reduced data sets could be analyzed, they first had to be scanned for errors introduced during the data collection process. Large anomalies introduced into the data due to signal interference, instrumentation difficulties, or data transmission problems can radically change calculations in means and standard deviations, introducing error into the data analyses. Datums which exhibited deviance greater than four standard deviations from the mean were replaced with an interpolated point.

This was a very small percentage of the total data points, usually less than 0.1%. Often, the data used had no anomalous points.

## Correlational Approach

Figure 8 shows the time histories of $C_n$ for 30% span, over each cycle for a 50 cycle set. $C_n$, the normal force, indicates what pressures and thus, loads, the blade is experiencing. A close inspection reveals that all cycles show a pressure deficit around 180° azimuth angle. Some cycles show the pressure drop a little earlier and some a little later than 180°. Some of the cycles have an additional pressure drop after the tower shadow and some have it before. There are also differences in the $C_n$ magnitudes within the cycles. Pearson's linear correlation coefficient, R, was used to quantify the similarities in the $C_n$ data from one cycle to another cycle within the same 50 cycle set. However, cycles which appeared to be very similar often had low correlations due to the high frequency noise of the signal. More representative correlations were achieved when some of the noise of the signal was first filtered.

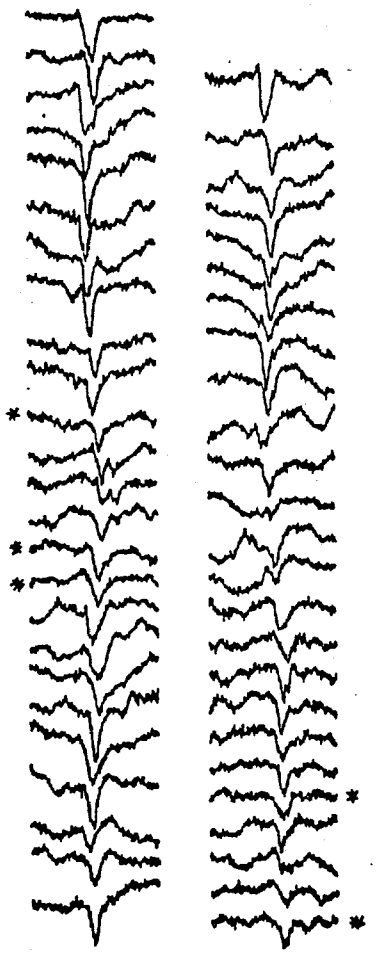

**Figure 8:** 50 consecutive individual cycles of $C_n$ data at 30% span with selected cycles that correlated above R = 0.8 highlighted with an asterisk.

To remove the signal noise, the data was filtered using a window averaging technique. This technique takes 5 data points on either side of the current point and averages the 11 points together. The average value is saved to be substituted for the current point. The "window" then moves down one point and averages that point with the 5 on both sides of it. The window moves in this way through the entire cycle.[3] The effect of the window averaging technique can be seen in Figure 9. The raw, unfiltered $C_n$ data of a single cycle is co-plotted with the filtered $C_n$. The two plots essentially track the same line even through the large pressure spike at 180° in the tower shadow region. The filtered cycles were then correlated with all other cycles within the same 50 cycle set. The window averaging technique improved the correlation of similar cycles.

Pearson's correlation coefficient was used to compare the cycles. Pearson's correlation coefficient, R, ranges from 1 to -1.[4] A value close to 1 indicates high correlations, a value close to 0 indicates no correlation, and -1 indicates similar cycles which are out of phase

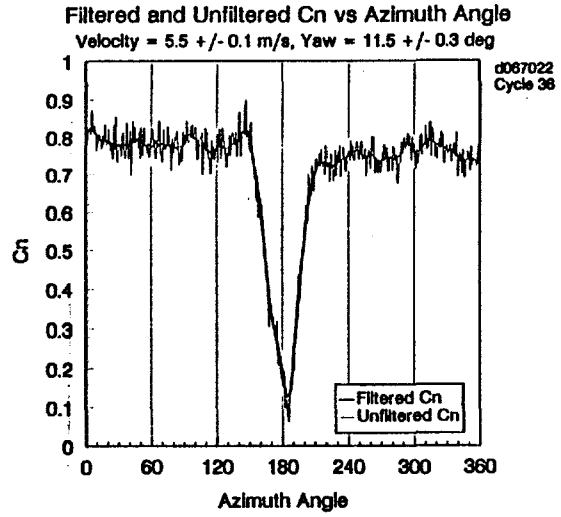


**Figure 9:** Single cycle of $C_n$ data showing the differences between the raw, unfiltered data and using the window averaging method.

by 180°. Cycles with a R of 0.8 or higher were considered to be highly correlated (based upon the 440 data points used). Figure 8, which shows the single rotational cycles at 30% span from one 50 cycle set has asterisks on one grouping of cycles which were highly correlated with each other. They all have the large pressure drop in about the same place and have similar slopes on the flatter parts of the curves. This 50 cycle data set also contains other groupings of cycles which correlate highly with each other but are not marked on this plot. All the subsets were plotted as a $C_n$ as a function of velocity plot, shown on Figure 10. The $C_n$ plot is a cycle average $C_n$ for those points in the 50 cycle set which were highly correlated. All five of the selected 50 cycle sets are represented. The values of $C_n$ are smallest at 80% span and increase inboard. The three outermost span locations, 47%, 63%, 80% seem to have the same general shape at lower velocities. 30% span, however, shows greater variance, especially above 11 m/s. The lower velocities, less than 8 - 9 m/s, show less variance.

## Consistent Inflow Approach

The second approach identified constant inflow conditions over three consecutive cycles. Three consecutive cycles with low standard deviations from the velocity and yaw indicated constant inflow conditions. Three cycle sets having a yaw between 1.5° and -1.5° with standard deviation within ±2.5° and velocity standard deviation within 10% of the mean velocity were used to create a reduced data set. The Cn averages for each three cycle set were plotted as a function of velocity, as was done for the correlational method. Figure 11 shows the results of the second approach. There are several similarities between these plots an the plots of Figure 10. Again, plots of spans 47%, 63% and 80% are similar to each other and 30% span seems to be operating in a different regime. There is not as much variance at higher velocities as there is in the correlational approach. The three cycle average plots are similar to the correlation plots. Figure 12 shows the three cycle average and correlation average Cn, co-plotted. The two methods track extremely well Thus, the same results were obtained through two different methods.

## Wind Tunnel and Field Data Comparison

In the wind tunnel, forces are defined as a function of angle of attack. Thus in order to compare our data to wind tunnel data, a conversion to angle of attack was necessary. Velocity of both methods was converted to angle of attack, using the formula previously given. The same $C_n$ data from the two methods was plotted as a function of angle of attack, shown in Figure 13. This graph shows the relationship between the rotating data and the

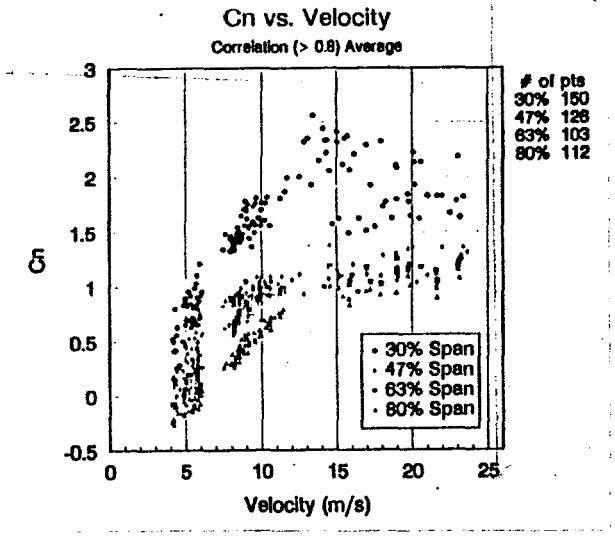


**Figure 10:** Plot of $C_n$ versus freestream velocity for all span locations obtained using the correlational method.

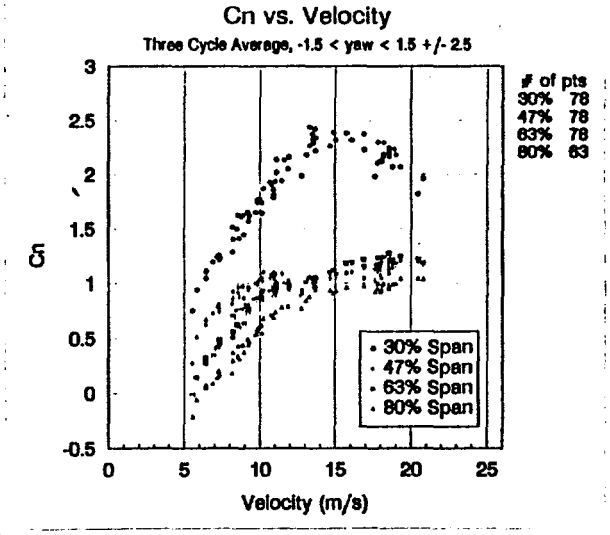


**Figure 11:** Plot of $C_n$ versus freestream velocity for all span locations obtained using the consistent inflow method.

wind tunnel curve, represented by a solid line. It shows there are three distinct operating regimes. The first regime is between 0° and approximately 14° angle of attack and corresponds to the linear portion of the wind tunnel curve. The second region is greater than 15° and includes only the outer three span locations. Within this region the $C_n$ values continue to increase beyond the wind tunnel static stall point. The third regime is greater than 15° for 30% span location. The $C_n$ linearly increases with no indication of stall until approximately 40° angle of attack. One possible reason for this occurrence is that a radically different flow environment exists for 30° span. The two methods, correlational and three cycle averaging, converged on the same $\alpha$ versus $C_n$ performance plot. Thus a cross-validated baseline performance curve for the aerodynamics of the turbine has been created.

## Summary

In order to improve wind energy performance, the aerodynamics of the turbine must be understood. A team of researchers is currently analyzing data gathered by NREL from the Combined Experiment. Various data reduction techniques were used to select consistent, reproducible data. Thus, a solid baseline has been established for the turbine performance in terms of cross-validated performance for different velocities. Although this is a recognizable achievement, much remains to be done. The next step is to compare anomalous events against this baseline to understand the causes of large transient loading which leads to problems and failures of the turbines.

## References

1. Butterfield, C.P., Musial, W.P., Simms, D.A., Combined Experiment Phase I Final Report, National Renewable Energy Laboratory, NREL/TP-257-4655, October 1992.

2. Butterfield, C.P., Nelson, E.N., Aerodynamic Testing of a Rotating Wind Turbine Blade, Solar Energy Research Institute, January, 1990.

3. Etter, D.M., Signal Processing: A Computer Approach, Prentice Hall, 1993.

4. Press, William H., Flannery, Brian P., Teukolsky, Saul A., Vetterling, William T., Numerical Recipes, The Art of Scientific Computing, Cambridge University Press, 1989.

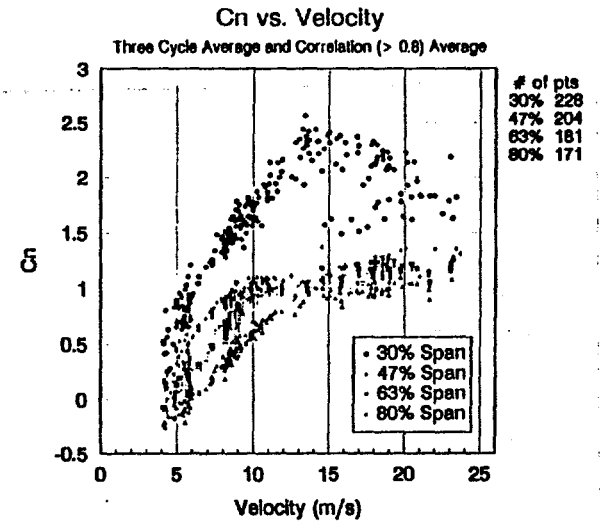


**Figure 12:** A comparison of the Cn versus velocity data from the correlational approach and the constant inflow approach showing the consistency of the two methods.

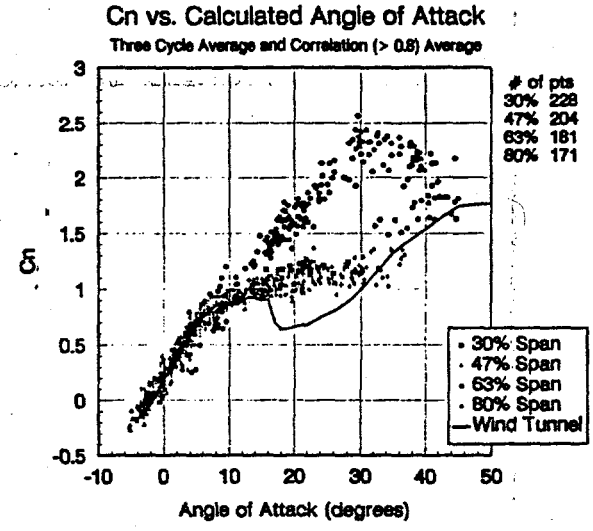


**Figure 13:** Plot of Cn versus effective angle of attack for all span locations using the data from both the correlational approach and the consistent inflow approach.